Efficient Bulk-Heterojunction Solar Cells Based on a Symmetrical D-π-A-π-D Organic Dye Molecule

ARTICLE *in* THE JOURNAL OF PHYSICAL CHEMISTRY C · JULY 2009

Impact Factor: 4.77 · DOI: 10.1021/jp902976w

6 AUTHORS, INCLUDING:

Bin Xu
Jilin University
95 PUBLICATIONS **1,901** CITATIONS

Efficient Bulk-Heterojunction Solar Cells Based on a Symmetrical D-π-A-π-D Organic Dye Molecule

Lili Xue, Jiating He, Xin Gu, Zhongfeng Yang, Bin Xu, and Wenjing Tian*

State Key Laboratory of Supramolecular Structure and Materials, Jilin University, Changchun 130012, P. R. China

Received: April 1, 2009; Revised Manuscript Received: May 25, 2009

A symmetrical D-π-A-π-D organic dye molecule 2-{2,6-bis-[2-(4-diphenylamino-phenyl)-vinyl]-pyran-4-ylidene}-malononitrile (DADP) has been introduced into solution-processable organic solar cells (S-P OSCs). Detailed investigations on the relationship between its molecular structure and thermal, photophysical, electrochemical properties and electronic structure are described. The optimized bulk heterojunction solar cell based on DADP as donor and PCBM as acceptor with the configuration of ITO/PEDOT/DADP:PCBM/LiF/Al exhibits a Voc of 0.98 V, Isc of 4.16 mA/cm^2, FF of 0.37, and power conversion efficiency (PCE) of 1.50% under the illumination of AM 1.5 simulated solar light (100 mW/cm^2). It was noted that the PCE of the device based on DADP is almost double that of the device based on TPA-DCM-TPA, an analogue of DADP, although there is only a small difference between their molecular structures; DADP has a shorter distance between the triphenylamine (TPA) group and the 2-pyran-4-ylidenemalonitrile (PM) group than TPA-DCM-TPA. This small structural difference results in a lower-lying highest occupied molecular orbital (HOMO) energy level and higher hole mobility in DADP, and ultimately leads to the increased PCEs of the DADP-based devices.

Introduction

Since the pioneering work of Tang in 1986,[1] remarkable advances have been made in organic solar cells (OSCs) over the past 20 years.[2] Up to now, a wide range of organic materials with distinct optoelectronic properties have been applied in OSCs mainly through two processing methods, namely, vacuum evaporation and spin-coating. It should be emphasized that, compared to inorganic silicon-based solar cells, the solution-processable OSCs (S-P OSCs) have attracted increasing attention in academia and industry because of their unique potential advantages such as easy fabrication, low cost, light weight, large area, and mechanical flexibility. To date, power conversion efficiencies (PCEs) approaching 5% on the basis of regioregular poly(3-hexylthiophene) (rr-P3HT) and [6,6]-phenyl-C61 butyric acid methyl ester fullerene derivative (PCBM) bulk heterojunction (BHJ) solar cells have been realized by optimizing the morphology of rr-P3HT in the active layer.[3] To further improve the performance of OSCs, design and synthesis of new materials remains a great challenge and will open novel opportunities in this active field.

To date, many π-conjugated donor−acceptor (D-A)-type small molecules, oligomers, and polymers have been synthesized and implemented in organic field-effect transistors (OFETs)[4] and organic light-emitting diodes (OLEDs)[5] as well as nonlinear optical (NLO) materials.[6] Theoretical and experimental advances in OSCs have demonstrated that such D−A-type small molecules and polymers have great potential as one class of promising materials in S-P OSCs.[7] On the one hand, the conjugated electron-donating and electron-accepting units combined through π-conjugated linkers have an intrinsic intramolecular charge transfer (ICT) character, reduce the optical band gap, and allow the absorption of the molecule to match well with the solar spectrum.[8] On the other hand, by flexible selection or modification of the donor and acceptor functional groups, desirable thermal properties, electronic structures, photoelectric properties, and solubility may be achieved.[9] In light of these considerations, a large number of novel low-bandgap D−A copolymers have been synthesized and applied in OSCs. For example, a series of electron-donating units such as fluorene,[10] carbazole,[11] dithieno[3,2-*b*:2′,3′-*d*]pyrrole (DTP),[12] and cyclopentadithiophene[13] have been copolymerized with many kinds of electron-accepting units such as benzothiadiazole (BTD)[14] and 4,7-dithien-2-yl-2,1,3-benzothiadiazole (DTBT),[15] etc. Among them, the PCE of the BHJ device based on poly[2,6-(4,4-bis-(2-ethylhexyl)-4*H*-cyclopenta[2,1-b;3,4-b_]-dithiophene)-*alt*-4,7-(2,1,3 benzothiadiazole)] (PCPDTBT) combined with C_{71}−PCBM can reach 5.5% by adding alkane dithiols to optimize the morphology of the active layer.[16] Compared with the D−A polymers, soluble D−A small molecules have the advantages of well-defined molecular structure, monodispersity, and relatively simple and reproducible synthesis and purification, making them ideal materials for S-P OSCs. However, the use of soluble D−A small molecules for S-P OSCs have been reported only by a few groups, and the PCEs based on soluble D−A small molecules are thus far limited between 0.81%[17] and 1.33%,[18] still unsuitable for commercial application. Although recent PCEs of 2.33% and 3.0% have been realized in S-P OSCs combining electron-poor diketopyrrolopyrrole (DPP)-containing low-dimensional oligothiophene as donors with PCBM or C_{71}−PCBM as acceptors,[19] exploiting appropriate D−A-type small molecule donor materials is still a great challenge for improving the performance of S-P OSCs.

DCM-type organic dyes are well known as low molecular weight red-emitting materials and have been intensively studied over the past two decades.[20−24] Actually, almost all DCM class red dyes have a D-π-A molecular structure that contains (dicyanomethylene)pyran (PM) as the electron acceptor. The

* Corresponding author. Tel: +86-431-85166368. Fax: +86-431-85193421. E-mail: wjtian@jlu.edu.cn.

10.1021/jp902976w CCC: $40.75
Published on Web 06/25/2009

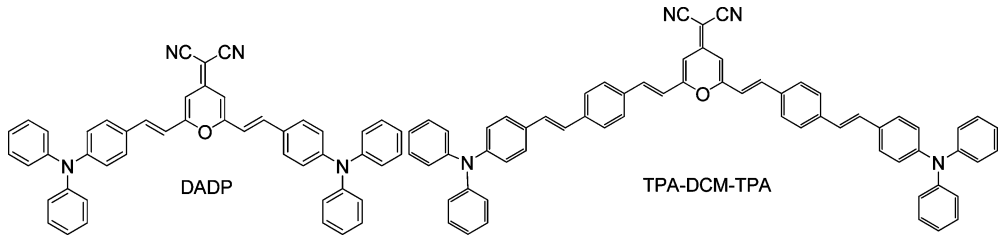

Figure 1. Chemical structure of DADP and TPA-DCM-TPA.

strong electron-withdrawing PM group can lower the lowest unoccupied molecular orbital (LUMO) energy level and extend the absorption band such that it nearly overlaps with the entire visible spectrum when combined with strong electron-donating units. Moreover, the strong intermolecular dipole−dipole interaction or intermolecular π-stacking of DCM-type organic dyes may be beneficial to the charge carrier transportation. Triphenylamine (TPA) is a unique molecule possessing 3D propeller-like geometry, glass-forming property, and relatively high oxidation potential as well as excellent hole-transporting property. The combination of electron-rich TPA and electron-deficient PM groups via π-conjugated spacers can effectively reduce the band gap and produce special physical and photoelectric properties. Li and co-workers have reported the synthesis of a symmetric D-(π-spacer)-A (π-spacer)-D-type small molecule, TPA-DCM-TPA, where two TPA groups are linked by divinylbenzene bridges at both ends of the PM group, and have successfully applied this material in S-P OSCs.[25] An analogous molecule, DADP, where two TPA groups are linked only by a vinyl bridge at both ends of the PM group, was first synthesized as a NLO material by Moylan et al.[26] and recently has shown promise as a red-emitting dopant for OLED applications.[27] The detailed molecular structures of DADP and TPA-DCM-TPA are shown in Figure 1. Although the synthesis and characterization of DADP as a NLO and red-emitting material have been reported as yet, there is a lack of systemic study on its thermal, photophysical, electrochemical, and electronic properties and application in S-P OSCs. In addition, the DADP molecule with its simple molecular structure can be regarded as a model compound for PM-based small molecules and polymers, and a deep understanding of its property−structure issues can bring us novel inspiration for the synthesis of new functional small molecules and polymers for S-P OSC applications.

In this article, we report the thermal, photophysical, electrochemical properties, and electronic structure of DADP in relation to its molecular structure and investigate DADP as donor combined with PCBM as acceptor in S-P OSCs applications. It was found that, compared with TPA-DCM-TPA-based OSCs, nearly 2-fold PCE of DADP-based OSCs is obtained due to a shorter distance between the TPA and PM moieties in the DADP molecule.

Experimental Section

Synthesis of DADP. DADP was synthesized on the basis of a Knoevenagel condensation reaction according to the literature.[26,27] The crude product was purified by recrystallization to afford a red-brown powder in a good yield of 80%. The structure of DADP was unequivocally confirmed by ^{1}H NMR and ^{13}C NMR measurements. DADP was obtained as a polycrystalline sample. The differential scanning calorimetry (DSC), to be presented and discussed in the following part, provides evidence for the polycrystalline state of the obtained DADP.

Photovoltaic Device Fabrication. The typical BHJ photovoltaic devices were fabricated in the following way. ITO glass (sheet resistance of 20 Ω sq^{-1}) serving as the transparent anode was routinely etched and then cleaned with detergent, acetone, and isopropyl alcohol in an ultrasonic bath boiled in H_2O_2, before being dried in an oven. A 50 nm layer of poly-[ethylene dioxy-thiophene]:(poly-(styrene sulfonic acid) (PEDOT:PSS) (Bayer PVP Al 4083) as a modified layer was then spin-coated onto the precleaned ITO glass substrate and then dried at 120 °C for 15 min in a vacuum oven. To investigate the effects of blend ratios on photovoltaic performance, the active layers were prepared from the chlorobenzene (CB) solutions of pristine DADP (10 mg/mL) or the DADP:PCBM blends with varied blend ratios (2:1, 1:1, 1:2, 1:3, 1:4 w/w) at a constant concentration of 20 mg/mL. Finally, LiF (1 nm) and Al (80 nm) were deposited onto the active layer by a conventional thermal evaporation method at a chamber pressure better than 5×10^{-4} Pa, providing devices with an active area of 2×2.5 mm^2. All device fabrications were performed in an ambient environment. The thicknesses of the active layers were measured on an Ambios Tech. XP-2 profilometer.

Measurements and Characterization. DSC measurements were performed on a NEZSCH (DSC-204) differential scanning calorimeter at 10 °C min^{-1} heating rate and 10 °C min^{-1}cooling rate under nitrogen atmosphere. UV−vis absorption and photoluminescence (PL) spectra were recorded on a Shimadzu UV-3100 Spectrometer and RF-5301PC spectrometer, respectively. Cyclic voltammetry (CV) measurement was carried out on a Bioanalytical Systems (BAS) 100B/W voltametric analyzer at a scanning rate of 100 mV s^{-1}, in which a three-electrode electrochemical cell was used including a platinum disk work electrode, a platinum wire auxiliary electrode, and a reference electrode Ag/AgCl. A 0.1 M solution of Bu_4NBF_4 in freshly distilled dichloromethane (CH_2Cl_2) was used as the supporting electrolyte and was flushed with N_2 prior to measurement to avoid oxygen contamination. The surface morphology of the photoactive layer was characterized using a Nanoscope IIIa Dimension 3100 atomic force microscopy (AFM) operating in the tapping mode. Current density−voltage ($J-V$) measurement of the devices was conducted on a computer-controlled Keithley 2400 SourceMeter measurement system. Air Mass 1.5 global (AM 1.5G) 100-mW/cm^2 illumination from a SCIENCETECH 500-W solar simulator acted as the light source. All of the measurements were performed under ambient atmosphere at room temperature.

Results and Discussion

Thermal Properties and Film Morphology of DADP. Figure 2 shows the DSC curves of DADP purified readily by recrystallization. When the sample was heated for the first cycle, an endothermic peak due to melting was observed at 288 °C, and then an amorphous glass was spontaneously formed via cooling back to 25 °C at a standard cooling rate of 10 °C min^{-1}. When the sample was heated for the second cycle, a glass-transition temperature (T_g) was observed at 132 °C. On further heating above T_g, an exothermic peak due to crystallization at

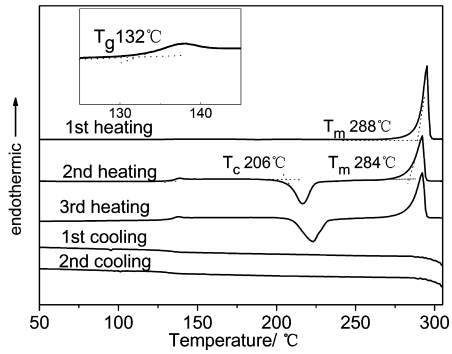

Figure 2. DSC curves of the obtained DADP polycrystal by recrystallization. Heating and cooling rates were 10 °C min^{-1}.

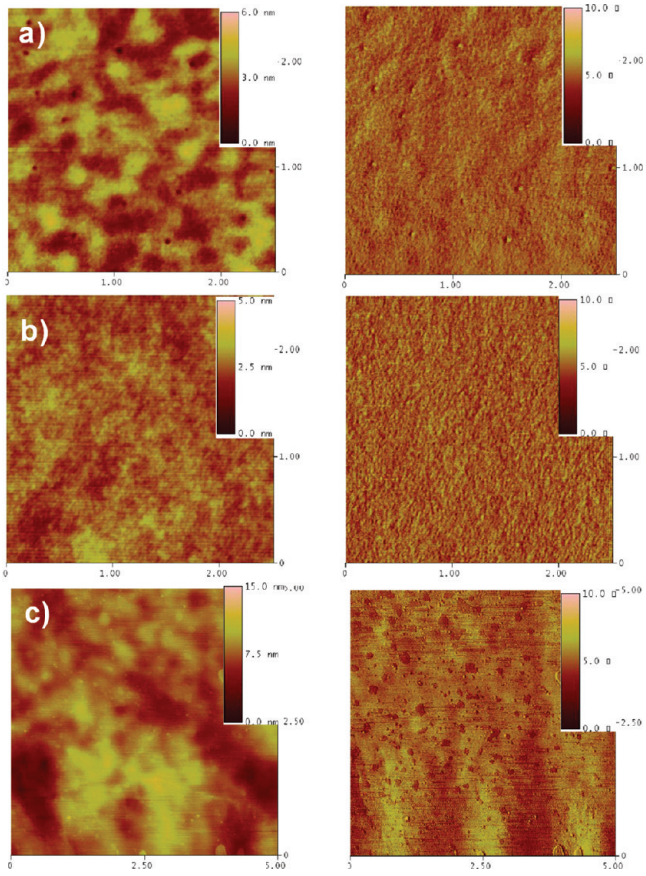

Figure 3. Topographic (left) and phase (right) images of pure DADP film cast from CF solution (a) and upon heating at 130 °C for 10 min (b) and at 160 °C for 10 min (c).

ca. 206 °C was observed, and then the crystal melted at 284 °C. Cooling scans did not exhibit major transitions. The similar DSC curves were reproduced repeatedly, and the T_g reading was constant during three such heating cycles. The DSC measurement confirms that DADP possesses excellent glass-forming properties above room temperature. Moreover, the incorporation of a structurally rigid PM moiety into the nonplanar DADP molecule enhances T_g[28] due to the reduced segmental motions and enhanced intermolecular dipolar interaction to a certain extent.

To gain more insight into the thermal properties of DADP molecules, AFM measurements were also performed. Figure 3 shows the evolution of topographic and phase images of pure DADP films cast from CF solution and annealing at different temperatures for 10 min. DADP film spin-coated from CF (Figure 3a) shows a smooth film (root-mean-square roughness (rms): 0.5 nm). A more flat film (rms: 0.25 nm) could be attained by annealing the pristine DADP film around T_g ca.130 °C for 10 min (Figure 3b), which is related to a conformational motion of the DADP molecule upon annealing. Rough film (rms: 1.2 nm) was formed with continued annealing for 10 min above T_g (160 °C selected in our case), and the large aggregations/crystal of DADP molecules could be clearly observed in the phase image (Figure 3c).

Photophysical Properties. The normalized optical absorption and photoluminescence (PL) spectra of DADP in solvents with varying polarity are shown in Figure 4, and the corresponding spectral data are summarized in Table 1. The absorption spectra of DADP in different solvents were characterized by three bands (Figure 4a). The first one located at 303 nm (not shown in the absorption plot) is the characteristic absorption peak of the TPA group that is not changed with the solvents. The second one around 360−370 nm can be assigned to a $\pi-\pi^*$ transition, which is also influenced little by the solvents. The third one, the most intense band peaking at 450−550 nm, is largely of ICT character and most sensitive to the solvents. In nonpolar solvents (such as petroleum ether and cyclohexane), the vibronic structure of the ICT absorption band is fairly well-resolved, but in polar solvents, the vibronic structure has completely disappeared. The ICT absorption peak wavelength is nearly solvent-polarity independent, suggesting a small interaction between the TPA-donor and the PM-acceptor in the ground state. In contrast, large positive solvatochromic behavior was observed in the PL spectra of DADP, in which bathochromic shifts of the emission bands occurred with increasing solvent polarity. In the nonpolar cyclohexane, DADP had a λ_{max}^{PL} of 519 nm with a distinct shoulder of 550 nm (full width at half-maximum (fwhm) = 30 nm). In the highly polar acetone, the vibronic structure of photoluminescence vanished, and the λ_{max}^{PL} red-shifts to as far as 627 nm (fwhm = 97 nm). On further increasing the polarity of solvents (acetonitrile, dimethyl formamide, and dimethyl sulfoxide), the PL emission was almost quenched, indicative of a complete charge-transfer electron state. The big differences in absorption and PL spectra imply that DADP has a very strong ICT character and that the excited-state energy level is influenced more than the ground-state energy level. Figure 5 displays the normalized UV−vis and PL spectra of DADP in dilute CB solution and as-prepared film cast from CB solution. Both absorption peaks in solution at 380 and 490 nm red-shift to 385 and 500 nm in film, indicating weak intermolecular interactions in the solid state due to the 3D steric structure of the TPA group. The characteristic absorption peak of the TPA group located at 303 nm is the same in solution and in film. However, the PL peak red-shifts from 590 nm in solution to 638 nm in film for DADP due to the strong dipole−dipole interaction in DADP molecules.

Theoretical Calculations. The ground-state geometry and the electron-state-density distribution of the highest occupied molecular orbital (HOMO) and LUMO of DADP have been fully optimized using density functional theory (DFT) based on the B3LYP/6-31G method as implemented in Gaussian 98[29] and illustrated in Figure 6. The calculation results demonstrate that the periplanatic PM moiety with its two adjacent phenyl vinyl units constitutes a large conjugated planar structure, and two diphenylamine units located at the end of the molecule result in an overall nonplanar structure for DADP. This nonplanar molecular structure could prevent crystallization resulting from the easy packing of molecules, favorably forming a homogeneous film.[30] Electron density of the HOMO distributes not only on the TPA-donor moieties but also on the PM-acceptor moiety,

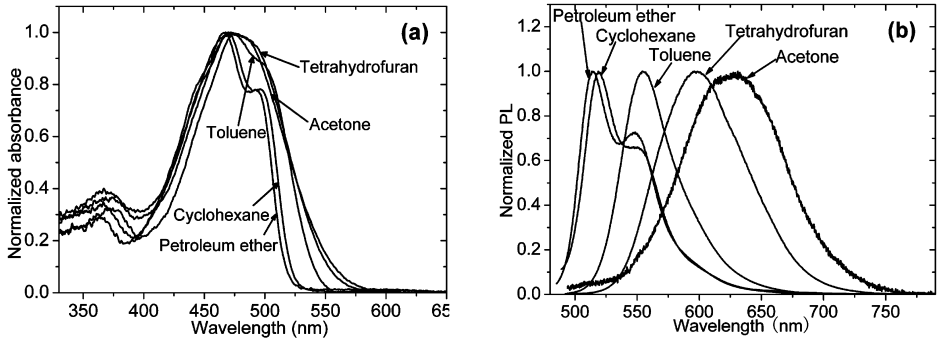

Figure 4. (a) Normalized optical absorption spectra and (b) PL spectra of DADP in solvents of various polarity, excited at the absorption maximum.

TABLE 1: Photophysical Data of DADP in Solvents of Various Polarity

solvent	λ_{max}^{UV} (nm)	λ_{max}^{PL} (nm)	fwhm (nm)
petroleum ether	465, 493	514, 549	29
cyclohexane	470, 497	519, 550	30
toluene	475, 500	555	51
tetrahydrofuran	480	598	84
acetone	480	627	97

while that of the LUMO mainly delocalizes on the PM-acceptor moiety, indicating a charge-transfer nature of HOMO → LUMO from the electron-donating N atom of the TPA moiety to the PM-acceptor moiety. The calculated HOMO and LUMO energies of the ground-state optimized geometry of DADP are −5.23 and −2.57 eV, respectively.

Electrochemical Properties. Cyclic voltammetry was performed to investigate the redox properties of DADP and estimate its HOMO and LUMO energy levels. As shown in Figure 7, in the positive scan, a reversible one-electron oxidation (p-doping) process of TPA takes place with the onset oxidation potential of 0.65 V vs Ag/AgCl. This lower oxidation potential compared with that of a single TPA unit (oxidation potential of 1.18 V in CH_2Cl_2)[31] may be attributed to the presence of the electron-withdrawing PM group, making the TPA more electrophilic and helping to stabilize the amine radical cation. In the negative scan, an irreversible one-electron reduction (n-doping) process takes place with the onset reduction potential of −1.18 V vs Ag/AgCl, which corresponds to the reduction of the PM moiety. The HOMO and LUMO energy levels obtained from electrochemical measurements are −5.28 and −3.45 eV, respectively. The HOMO energy level is in agreement with the DFT calculated value. Although there is some divergency of LUMO energy levels between the experimental and calculated values, the experimental value of the LUMO is similar to that of the PM-containing polymers.[32] Both the HOMO and LUMO energy levels of DADP are proper for BHJ solar cells when PCBM is used as the electron acceptor.

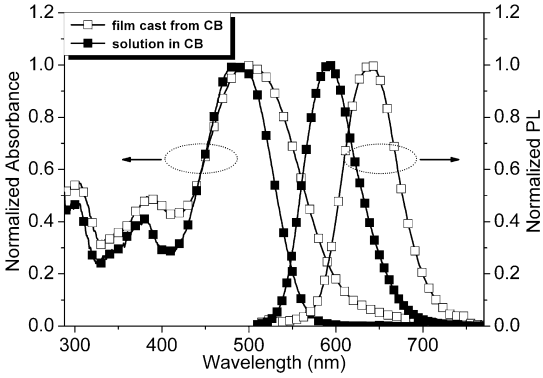

Figure 5. Normalized UV−vis and PL spectra of DADP in dilute CB solution and as-prepared film cast from CB solution.

Hole Mobility Measurements. Charge carrier mobility is an important parameter for materials used in OSCs. Hole mobility in pure DADP was determined by the space-charge limited current method[33] with a device structure of ITO/PEDOT:PSS/DADP/Au. As shown in Figure 8, the result was plotted as $\ln[JL^3/(V_{appl}-V_{bi})^2]$ vs $(V_{appl}-V_{bi})^{0.5}$.[25] The analysis of the SCLC experiment gives a hole mobility of 1.38×10^{-5} cm^2/V^{-1} s^{-1} at room temperature.

Photovoltaic Performance and Morphology of the Active Layers. It is known that the solvent used in spin-coating significantly affects the photovoltaic performance. Although DADP dissolves easily in a strong polar CF solvent in contrast to a weak polar CB, in our experiments, CB was selected for the device preparation owing to the following two factors: (1) During the spin-coating process of a pristine DADP film, the easy evaporation of CF produces a film with a lot of pinholes that are very undesirable in the PV device, as shown in Figure 3a. In comparison, the slow evaporation of CB tends to produce pinhole-free uniform films. (2) CB is an excellent solvent for PCBM with dissolved concentration up to 42 mg/mL.[34]

Devices based on pure DADP and varied blend ratios of DADP:PCBM (2:1, 1:1, 1:2, 1:3, 1:4) have been prepared, and the active layer thicknesses of various devices have been optimized. We found that 55−65 nm is the best thickness for all kinds of devices except that 35 nm is the best for the single layer DADP device. The current density versus voltage ($J-V$) curves measured for all devices are shown in Figure 9, and the performance parameters of the devices are listed in Table 2. The single layer DADP device shows a high open-circuit voltage (Voc) of 1.26 V, low short-circuit current (Isc) of 0.35 mA/cm^2, fill factor (FF) of 0.21, and a PCE of only 0.092%. For the BHJ devices, when the blend ratio of DADP and PCBM varied from 2:1 to 1:4, the Voc shows a gradual decrement trend from 1.08 to 0.92 V, but the FF increases from 0.21 to 0.40 with an increasing PCBM ratio. The lowest FF of the single layer DADP device suggests that the ICT state in DADP molecules cannot efficiently dissociate and transport the charges to the electrodes, while the charge recombination still exists. By adding the PCBM into the DADP matrix, the device can benefit from the ultrafast and complete intermolecular charge transfer between DADP and PCBM; in this way, the charge recombination is suppressed, and greatly improved Isc and FF are obtained. However, devices with higher PCBM ratio inevitably lead to a tendency that some PCBM domains contact with the anode PEDOT layer and then induce a reverse electron flow from LiF/Al to PEDOT, resulting in a reduced Voc.[35]

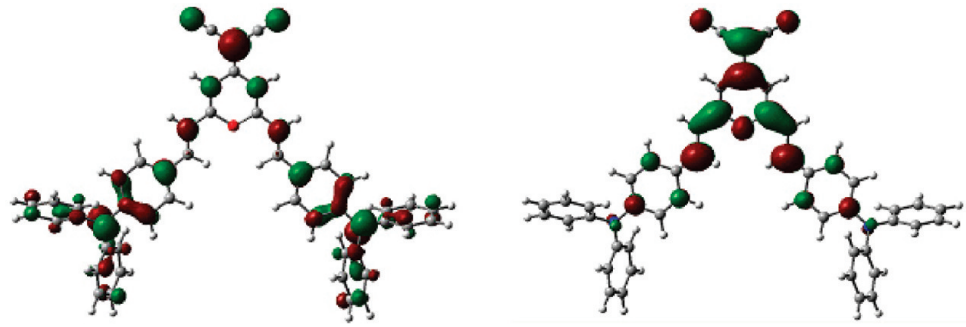

Figure 6. HOMO and LUMO orbitals of DADP in its optimized ground-state structures.

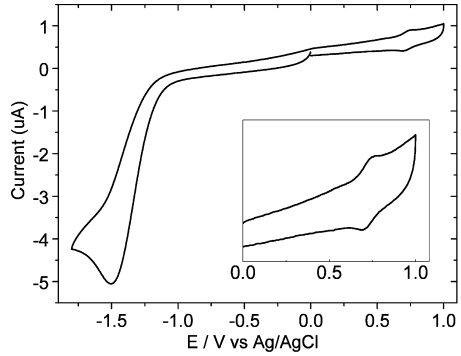

Figure 7. CV curve of DADP in dichloromethane/Bu_4NPF_6 (0.1 M) at a scan rate of 100 mV/s.

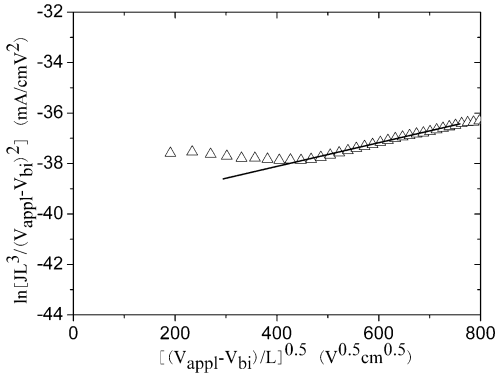

Figure 8. $J-V$ curve from the device ITO/PEDOT:PSS/DADP/Au, plotted from $\ln(JL^3/V^2)$ vs $(V/L)^{0.5}$ according to the SCLC model equation where J is the current density, L is the thickness of the polymer layer, and V is the voltage.

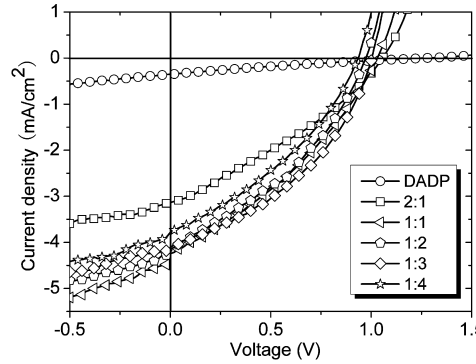

Figure 9. $J-V$ curves of the devices based on DADP:PCBM with different blend ratios (1:0, 1:0.5, 1:1, 1:2, 1:3, 1:4, w/w) under the illumination of AM 1.5, 100 mW/cm^2.

TABLE 2: Device Parameters of ITO/PEDOT:PSS/ DADP:PCBM/LiF/Al Solar Cells with Different Blend Ratios

DADP:PCBM blending ratio	Voc (V)	Isc (mA/cm^2)	FF	PCE (%)
DADP	1.26	0.35	0.21	0.092
2:1	1.06	3.13	0.32	1.05
1:1	1.04	4.25	0.34	1.49
1:2	0.98	4.16	0.37	1.50
1:3	0.94	3.97	0.40	1.48
1:4	0.94	3.79	0.37	1.25

Interestingly, the best PCEs around 1.50% were simultaneously obtained in BHJ devices with blend ratios of 1:1, 1:2, and 1:3. It can be envisioned that such D−A small molecules would reduce the amount of acceptor material such as PCBM when it is used as the donor in BHJ OSCs.

Given that the morphology of the photoactive layer is another important factor that influences photovoltaic performance, we analyzed the morphology of pristine DADP films and DADP/PCBM blend films with varied blend ratios by AFM. The images in Figure 10 reveal that the pristine DADP film has the most smooth surface with a root-mean-square roughness (rms) of 0.35 nm. All blend films are coarser than the pristine film. rms for the blend films with various blend ratios of 1:0.5, 1:1, 1:2, 1:3, 1:4 are 0.56, 0.74, 0.56, 0.67, and 0.72, respectively. All of these films are homogeneous with nanoscale phase separation, as a result of the good miscibility of DADP and PCBM molecules.

A comparison of the performances of the devices based on DADP and TPA-DCM-TPA is listed in Table 3. We can see that devices based on DADP show higher Voc, Isc, and PCE than those based on TPA-DCM-TPA, which can be related to the differences in molecular structures.

As shown in Figure 1, in the DADP molecule, each TPA group is connected by a vinyl-spacer at both ends of the PM group, while in the TPA-DCM-TPA molecule, additional phenyl vinyl units were included in the π-spacer. Thus, there is a shorter linker between the TPA and PM groups in DADP than in TPA-DCM-TPA. This small structural difference has a significant impact on the HOMO and LUMO energy levels of DADP and TPA-DCM-TPA. Both the HOMO and LUMO of DADP (−5.28 and −3.45 eV) are lower-lying compared to that of TPA-DCM-TPA (−5.14 and −2.76 eV).[25] Since the Voc in BHJ devices using PCBM as acceptor is mainly determined by the HOMO level of the donor and LUMO level of the acceptor,[36] the energy difference of 0.14 eV in HOMO levels between DADP and TPA-DCM-TPA is in agreement with the ultimate Voc of devices based on DADP and TPA-DCM-TPA.

On the other hand, such a small structure difference has a remarkable impact on charge transfer. In the DADP molecule, as discussed above, the electron density of the HOMO is distributed over the whole molecule; HOMO → LUMO excitation moves the electron distribution mainly on the PM moiety. This effective ICT process indicates that the electron transfer

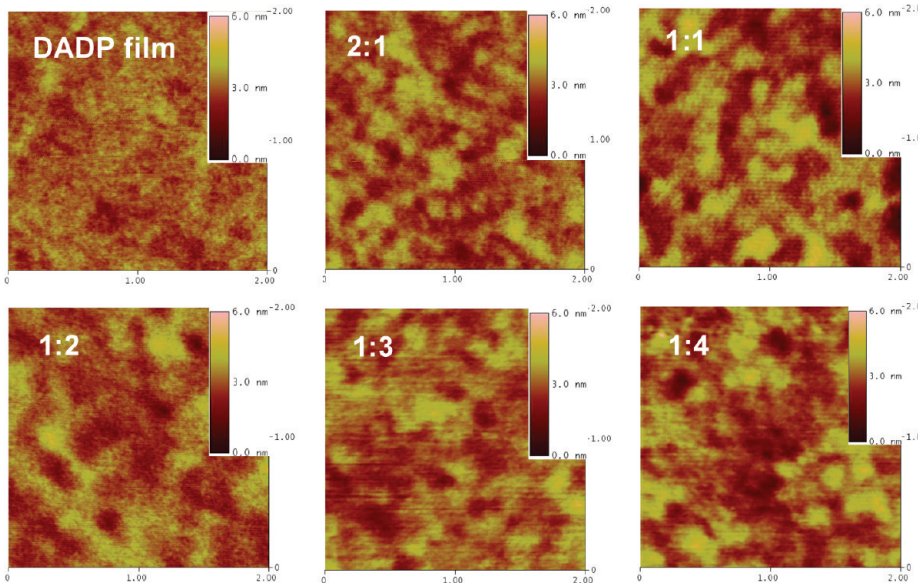

Figure 10. AFM topography images (2 μm × 2 μm) of a pristine DADP film and DADP:PCBM blend films (1:0.5, 1:1, 1:2, 1:3, 1:4, w/w) cast from CB solutions.

TABLE 3: Comparison of the Device Performance of DADP and TPA-DCM-TPA BHJ Photovoltaic Devices with Similar Device Structure ITO/PEDOT:PSS/Small molecules:PCBM/Cathode[a]

devices (blend ratio)	Voc (V)	Isc (mA/cm^2)	FF (%)	PCE (%)
1/2 (1:0)	1.26/0.86	0.35/0.039	21/29	0.092/0.01
1/2 (2:1)	1.06/0.90	3.13/1.43	32/30	1.05/0.32
1/**2** (1:1)	1.04/0.90	4.25/1.69	34/37.4	1.49/0.57
1/**2** (1:2)	0.98/0.75	4.16/2.02	37/39.5	1.50/0.60
1/**2** (1:3)	0.94/0.90	3.97/2.14	40/41.3	1.48/0.79
1/**2** (1:4)	0.92/0.69	3.76/1.4	36/34.5	1.25/0.33

[a] **1**, DADP- or DADP:PCBM-based devices with LiF/Al as cathode; **2**, TPA-DCM-TPA-based devices with LiF/Al as cathode; TPA-DCM-TPA:PCBM-based devices with Ba/Al as cathode.

from the excited DADP molecules to the PCBM acceptors is feasible. In the TPA-DCM-TPA molecule, the electron density of the HOMO orbital is mainly located on the TPA units with some extending to adjacent vinyl phenyl units; however, due to a longer divinylphenyl linker between TPA-donor and PM-acceptor moieties in TPA-DCM-TPA, HOMO → LUMO excitation moves the electron density distribution not only on the PM moiety but also partially on the divinylphenyl linkers.[25] Therefore, in the TPA-DCM-TPA molecule, partial negative charges on the divinylphenyl linker leads to a trap for charge transfer, further influencing the charge transfer from the PM moiety to the PCBM acceptors. This phenomenon is similar to a serious of triphenylamine dyes containing a cyanovinyl moiety in the π-spacer recently reported by Tian et al.[37] and Huang et al.[38]

Moreover, the hole mobility of DADP (1.38×10^{-5} cm2/V^{-1} s^{-1}) is 1 order of magnitude higher than that of TPA-DCM-TPA (1.19×10^{-6} cm^2/V^{-1} s^{-1}),[25] which leads to the relatively high photovoltaic performance of DADP-based devices. This improved hole mobility is reflected in the photovoltaic properties of single layer DADP- and TPA-DCM-TPA-based devices, as shown in Table 3. The single layer DADP-based device shows a Voc of 1.26 V, an Isc of 0.35 mA/cm^2, an FF of 0.21, and a PCE of 0.092%. Both the Isc and PCE are nearly 10-fold higher than those of a single layer TPA-DCM-TPA-based device due to the higher hole mobility of DADP.

Conclusions

In summary, a symmetrical D-π-A-π-D dye molecule DADP has been employed as a donor material for S-P OSC applications. The combination of the nonplanar TPA groups and strong electron-withdrawing PM group with a shorter π-spacer makes DADP a promising donor material for application in S-P OSCs, with high Voc of about 1 V and PCE of 1.50%. This work suggests that D-π-A-π-D small molecules with simple molecular structures, extended absorption bands, and high carrier mobility will be one class of promising materials for high-performance S-P OSC applications.

Acknowledgment. This work was supported by State Key Development Program for Basic Research of China (973 program, 2009CB623605), National Natural Science Foundation of China (50673035, 20874305), Program for the Changjiang Scholars and Innovative Research Team in University (IRT0422), Program for New Century Excellent Talents in Universities of China Ministry of Education, 111 Project (B06009), and Key Project of Jilin Province (20080305).

References and Notes

(1) Tang, C. W. *Appl. Phys. Lett.* **1986**, *48*, 183.

(2) (a) Sariciftci, N. S.; Smilowitz, L. S.; Heeger, A. J.; Wudl, F. *Science* **1992**, *258*, 1474. (b) Yu, G.; Gao, J.; Hummelen, J. C.; Wudl, F.; Heeger, A. J. *Science* **1995**, *270*, 1789. (c) Shaheen, S. E.; Brabec, C. J.; Sariciftci, N. S.; Padinger, F.; Fromherz, T.; Hummelen, J. C. *Appl. Phys. Lett.* **2001**, *78*, 841. (d) Padinger, F. R.; Rittberger, S.; Sariciftci, N. S. *Adv. Funct. Mater.* **2003**, *13*, 1.

(3) (a) Ma, W.; Yang, C.; Gong, X.; Lee, K.; Heeger, A. J. *Adv. Funct. Mater.* **2005**, *15*, 1617. (b) Li, G.; Shrotriya, V.; Huang, J.; Yao, Y.; Moriarty, T.; Emery, K.; Yang, Y. *Nat. Mater.* **2005**, *4*, 864.

(4) (a) Kulkarni, A. P.; Zhu, Y.; Babel, A.; Wu, P. T.; Jenekhe, S. A. *Chem. Mater.* **2008**, *20*, 4212. (b) Chen, M. X.; Perzon, E.; Robisson, N.; Jönsson, S. K. M.; Andersson, M. R.; Fahlman, M.; Berggren, M. *Synth. Met.* **2004**, *14*, 6–233.

(5) (a) Huang, J.; Niu, Y.; Yang, W.; Mo, Y.; Yuan, M.; Cao, Y. *Macromolecules* **2002**, *35*, 6080. (b) Li, J.; Liu, D.; Hong, Z.; Tong, S.; Wang, P.; Ma, C.; Lengyel, O.; Lee, C. S.; Kwong, H. L.; Lee, S *Chem. Mater.* **2003**, *15*, 1486. (c) Huang, J.; Qiao, X.; Xia, Y.; Zhu, X.; Ma, D.; Cao, Y.; Roncali, J. *Adv. Mater.* **2008**, *20*, 1.

(6) (a) Borbone, F.; Caruso, U.; Diana, R.; Panunzi, B.; Roviello, A.; Tingoli, M.; Tuzi, A. *Org. Electron.* **2009**, *10*, 53. (b) Ravindra, H. J.; Kiran, A. J.; Dharmaprakash, S. M.; Rai, N. S.; Chandrasekharan, K.; Kalluraya, B.; Rotermund, F. *J. Cryst. Growth* **2008**, *310*, 4169.

(7) (a) Mataga, N.; Chosrowjan, H.; Taniguchi, S. *J. Photochem. Photobiol.* **2005**, *6*, 37. (b) Hou, J.; Park, M.; Zhang, S.; Yao, Y.; Chen, L.; Li, J.; Yang, Y. *Macromolecules* **2008**, *41*, 6012.

(8) Colladet, K.; Fourier, S.; Cleij, T. J.; Lutsen, L.; Gelan, J.; Vanderzande, D.; Nguyen, L. H.; Neugebauer, H.; Sariciftci, S.; Aguirre, A.; Janssen, G.; Goovaerts, E. *Macromolecules* **2007**, *40*, 65.

(9) Zhang, C.; Choi, S.; Haliburton, J.; Cleveland, T.; Li, R.; Sun, S.; Ledbetter, A.; Bonner, C. E. *Macromolecules* **2006**, *39*, 4317.

(10) Mammo, W.; Admassie, S.; Gadisa, A.; Zhang, F.; Inganäs, O.; Andersson, M. R. *Sol. Energy Mater. Sol. Cells* **2007**, *91*, 1010.

(11) Blouin, N.; Michaud, A.; Leclerc, M. *Adv. Mater.* **2007**, *19*, 2295.

(12) Zhou, E.; Nakamura, M.; Nishizawa, T.; Zhang, Y.; Wei, Q.; Tajima, K.; Yang, C.; Hashimoto, K. *Macromolecules* **2008**, *41*, 8302.

(13) Soci, C.; Hwang, I. W.; Moses, D.; Zhu, Z.; Waller, D.; Gaudiana, R.; Brabec, C. J.; Heeger, A. J. *Adv. Funct. Mater.* **2007**, *17*, 632.

(14) Hou, J.; Chen, H.; Zhang, S.; Li, G.; Yang, Y. *J. Am. Chem. Soc.* **2008**, *130*, 16144.

(15) Liao, L.; Dai, L. M.; Smith, A.; Durstock, M.; Lu, J. P.; Ding, J. F.; Tao, Y. *Macromolecules* **2007**, *40*, 9406.

(16) Peet, J.; Kim, J. Y.; Coates, N. E.; Ma, W. L.; Moses, D.; Heeger, A. J.; Bazan, G. C. *Nat. Mater.* **2007**, *6*, 497.

(17) Roquet, S.; Cravino, A.; Leriche, P.; Alévêque, O.; Frère, P.; Roncali, J. *J. Am. Chem. Soc.* **2006**, *128*, 3459.

(18) He, C.; He, Q.; Yi, Y.; Wu, G.; Yang, C.; Bai, F.; Shuai, Z.; Wang, L.; Li, Y. *J. Mater. Chem.* **2008**, *18*, 4085.

(19) (a) Tamayo, A. B.; Walker, B.; Nguyen, T. Q. *J. Phys. Chem. C* **2008**, *112*, 11545. (b) Tamayo, A. B.; Dang, X. D.; Walker, B.; Seo, J.; Kent, T.; Nguyen, T. Q. *Appl. Phys. Lett.* **2009**, *94*, 103301.

(20) Meyer, M.; Mialocq, J. C.; Perly, B. *J. Phys. Chem.* **1990**, *94*, 98.

(21) Pal, S. K.; Sukul, D.; Mandal, D.; Bhattacharyya, K. *J. Phys. Chem. B* **2000**, *104*, 4529.

(22) Jung, B. J.; Yoon, C. B.; Shim, H. K.; Do, L. M.; Zyung, T. *Adv. Funct. Mater.* **2001**, *11*, 430.

(23) Jung, B. J.; Lee, J. I.; Chu, H. Y.; Do, L. M.; Lee, J.; Shim, H. Ku. *J. Mater. Chem.* **2005**, *15*, 2470.

(24) Yao, Y. S.; Zhou, Q. X.; Wang, X. S.; Wang, Y.; Zhang, B. W. *Adv. Funct. Mater.* **2007**, *17*, 93.

(25) He, C.; He, Q.; Yang, X.; Wu, G.; Yang, C.; Bai, F.; Shuai, Z.; Wang, L.; Li, Y. *J. Phys. Chem. C* **2007**, *111*, 8661.

(26) Moylan, C. R.; Ermer, S.; Lovejoy, S. M.; McComb, I. H.; Leung, D. S.; Wortmann, R.; Krdmer, P.; Twieg, R. J. *J. Am. Chem. Soc.* **1996**, *118*, 12950.

(27) Swanson, S. A.; Wallraff, G. M.; Chen, J. P.; Zhang, W.; Bozano, L. D.; Carter, K. R.; Salem, J. R.; Villa, R.; Scott, J. C. *Chem. Mater.* **2003**, *15*, 2305.

(28) Shirota, Y. *J. Mater. Chem.* **2000**, *10*, 1.

(29) Becke, A. D. *J. Chem. Phys.* **1993**, *98*, 5648.

(30) Cravino, A.; Leriche, P.; Alévêque, O.; Roquet, S.; Roncali, J. *Adv. Mater.* **2006**, *18*, 3033.

(31) Yeh, S. J.; Tsai, C. Y.; Huang, C. Y.; Liou, G. S.; Cheng, Sh. H. *Electrochem. Commun.* **2003**, *5*, 373.

(32) Kim, J. H.; Lee, H. *Chem. Mater.* **2002**, *14*, 2270.

(33) Malliaras, G. G.; Salem, J. R.; Brock, P. J.; Scott, C. *Phys. Rev. B* **1998**, *58*, 13411.

(34) Hoppe, H.; Niggemann, M.; Winder, C.; Kraut, J.; Hiesgen, R.; Hinsch, A.; Meissner, D.; Sariciftci, N. S. *Adv. Funct. Mater.* **2004**, *14*, 1005.

(35) Xue, L.; Liu, L.; Gao, Q.; Wen, S.; He, J.; Tian, W. *Sol. Energy Mater. Sol. Cells* **2009**, *93*, 501.

(36) Scharber, M. C.; Mühlbacher, D.; Koppe, M.; Denk, P.; Waldauf, C.; Heeger, A. J.; Brabec, C. J. *Adv. Mater.* **2006**, *18*, 789.

(37) Tian, H.; Yang, X.; Chen, R.; Zhang, R.; Hagfeldt, A.; Sun, L. *J. Phys. Chem. C* **2008**, *112*, 11023.

(38) Huang, S. T.; Hsu, Y. C.; Yen, Y. S.; Chou, H. H.; Lin, J. T.; Chang, C. W.; Hsu, C. P.; Tsai, C.; Yin, D. J. *J. Phys. Chem. C* **2008**, *112*, 19739.

JP902976W